J Fluoresc (2009) 19:317–326
DOI 10.1007/s10895-008-0418-y

ORIGINAL PAPER

Thermodynamics, Conformation and Active Sites of the Binding of Zn–Nd Hetero-bimetallic Schiff Base to Bovine Serum Albumin

Qi Xiao · Shan Huang · Yi Liu · Fang-fang Tian · Jun-cheng Zhu

Received: 14 April 2008 / Accepted: 11 September 2008 / Published online: 21 October 2008

Abstract The interactions between *N*,*N*′-di(2-hydroxy-3-methyoxy-phenyl-1-methylene)-*o*-phenyldiamine-mone Zn (II), Nd(III) nitrate (2LZnNd) and bovine serum albumin (BSA) was investigated by various spectroscopic techniques under physiological conditions. It was proved that the fluorescence quenching of BSA by 2LZnNb was a result of the formation of a non-fluorescent complex with the binding constants of 3.15×10^5; 2.72×10^5 and 2.44×10^5 M^{-1} at 298 K, 304 K and 310 K, respectively. A marked increase in the fluorescence anisotropy in the proteinous environments indicates that BSA introduces motional restriction on the drug molecule. The corresponding thermodynamics parameters ΔH and ΔS were calculated to be –16.36 kJ mol^{-1} and 43.48 J mol^{-1} K^{-1} via van't Hoff equation. Moreover, the competitive probes experiment revealed that the binding location of 2LZnNb to BSA is in the hydrophobic pocket of site II. The effect of 2LZnNb on the conformation of BSA has been analyzed by means of CD spectrum and three-dimensional fluorescence spectra. The results indicate that the conformation of BSA molecules was changed in the presence of 2LZnNb Schiff base.

Keywords Bovine serum albumin · Circular dichroism · Competitive probe · Schiff base · Thermodynamic parameters

Q. Xiao · Y. Liu (✉) · F.-f. Tian · J.-c. Zhu
State Key Laboratory of Virology,
College of Chemistry and Molecular Science, Wuhan University,
Wuhan 430072, People's Republic of China
e-mail: prof.liuyi@263.net

S. Huang
Research Center of Analytical Science,
College of Chemistry and Molecular Sciences, Wuhan University,
Wuhan 430072, People's Republic of China

Introduction

The Schiff-base has been approbated with excellent anti-tumor [1–3] and antibacterial properties [4–7]. A series of Schiff-bases were synthesized to develop the potential drugs for purposes of diminishing inflammation and curing cancer. Lanthanide coordination compounds have also exhibited excellent biological effect as active agents in cancer radiotherapy [8], as antibacterial and anti-tumor pharmaceutical [9–11]. Particular attention has recently been paid to the synthesis and bioactivity study of both transition metals and lanthanide with Schiff-base ligand and their derivates. This is due to their uses as biological models in understanding the structure of biomolecules and biological processes [12–14], and also the coordination ability of transition metals and lanthanide could enhance the bioactivity of Schiff-base complexes. *N*,*N*′-di(2-hydroxy-3-methyoxy-phenyl-1-methylene)-*o*-phenyldiamine-mone Zn(II), Nd(III) nitrate (2LZnNd, see Fig. 1C) was hetero-bimetallic complex contained both transition metal (zinc) and lanthanide (neodymium) with Schiff-base ligand. However, only a few studies investigated the responses of biological systems to Zn–Nd bimetallic Schiff base in detail, and there are also very few overall conceptual frameworks. For example, Boghaei *et al.* reported on the interaction of copper (II) complex of compartmental Schiff base ligand with bovine serum albumin by using circular dichroism spectroscopy and cyclic voltammetry, the results indicated that the interaction leaded to changes in the secondary structure of BSA [15]. In another study, Shrivastava *et al.* showed that binding of the Schiff-base ligand to BSA resulted in a remarkable change of the helicity content with a large binding constant [16].

Serum albumins, abundant in the blood plasma, are the most widely studied proteins act as transportation and disposition of endogenous and exogenous compounds [17–19]. Albumins

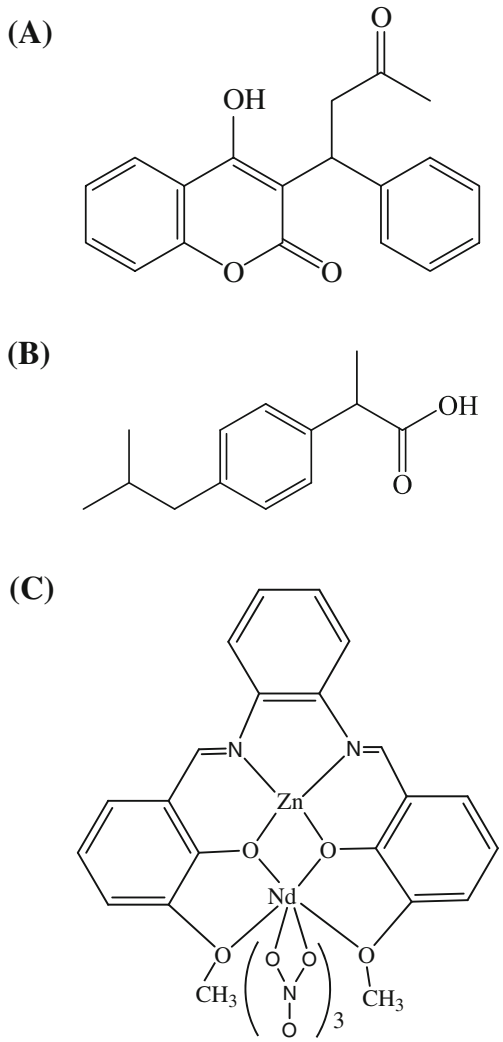

Fig. 1 Molecular structure of **a** warfarin, **b** ibuprofen and **c** 2LZnNd

have been identified as major transport proteins in blood plasma for many compounds such as fatty acids, amino acids, diverse range of metabolites, drugs and organic compound [20–22]. More and more clinical and pharmaceutical interests in serum albumins derive from their effects on the drug of pharmacokinetics when bound to serum albumins. In this work, BSA is selected as our protein model because of its low cost, ready availability, unusual ligand-binding properties. The results of all the studies are consistent with the fact that bovine and human serum albumins are homologous proteins [23, 24].

We report here this unprecedent study of interaction between 2LZnNd and BSA under physiological condition. In order to determine the affinity of 2LZnNd to BSA, we planned to carry out detailed investigation of BSA–2LZnNd association using fluorescence spectroscopy, fluorescence anisotropy, and UV–Vis absorption spectrum. The binding site of 2LZnNd to BSA was done by employing the known probe of warfarin and ibuprofen. Additionally, the conformational changes of BSA induced by 2LZnNd were estimated by circular dichroism and three-dimensional fluorescence spectra. This study may provide valuable information to the growing concern regarding the biological action of novel bimetallic Schiff base introduced to organism.

Materials and methods

Materials

N,*N*′-di(2-hydroxy-3-methyoxy-phenyl-1-methylene)-*o*-phenyldiamine-mone Zn(II), Nd(III) nitrate (2LZnNd) was synthesized and characterized according to the literature [25] and prepared by DMF. The structures are shown in Fig. 1. Bovine serum albumin (BSA, fatty acid free) was purchased from Sigma. BSA was dissolved in 0.1 M Phosphate Buffered Saline (PBS) (pH 7.4±0.1). The concentration of the protein was determined spectrophotometrically using an extinction coefficient (ε=280) of 36 600 M^{-1} cm^{-1}. Warfarin, obtained from Medicine Co. Ltd. of Jiangsu in China. Ibuprofen, presented by the company of Hubei Biocause Heilen Pharmaceutical Co. Ltd. in China. All other reagents were was purchased from Sigma Aldrich (St. Louis, MO, USA) and used as purchased without further purification. All solutions were prepared with doubly distilled water.

Fluorescence measurements

All fluorescence spectra were recorded on F-2500 fluorophotometer (Hitachi, Japan) equipped with a Xenon lamp excitation source and a thermostat bath. Fluorescence spectra were recorded at 298 K, 304 K, 310 K in the range of 290–450 nm and the width of the excitation and emission slit were set to 5.0 and 5.0 nm. An excitation wavelength of 285 nm was chosen and very dilute solutions were used in the experiment (BSA 2.0 μM, 2LZnNd in the range of 0–5.0 μM) to avoid inner filter effect. The quenching effect of DMF was evaluated and the result showed that the effect of DMF on the quenching of BSA could be negligible in the amount used.

The three-dimensional fluorescence spectrum was performed under the following conditions: the emission wavelength was recorded between 200 and 500 nm, the initial excitation wavelength was set to 200 nm with increment of 5 nm, the number of scanning curves was 31, other scanning parameters were just the same to that of the fluorescence quenching spectrum, c (2LZnNd)=c (BSA)=2 μM.

Fluorescence anisotropy measurement

Steady-state fluorescence polarization measurements were performed with an automatic polarization device of LS55

spectrofluorometer (Perkin Elmer, USA) at room temperature. Steady-state anisotropy, r, is defined by [26]:

$$r = (I_{VV} - GI_{VH})/(I_{VV} + 2GI_{VH}) \quad (1)$$

$$G = I_{VH}/I_{VV} \quad (2)$$

where I_{VV} and I_{VH} are the intensities obtained with the excitation polarizer oriented vertically and the emission polarizer oriented vertically and horizontally, respectively. G is the instrument grating correction factor. All of the anisotropy measurements were performed at room temperature. Excitation and emission bandwiths were all adjusted to 5 nm. Each titration point of the sample equilibration at least three times with an integration time of 1 min was collected. The fluorescence anisotropy of the interaction between 2LZnNd and BSA was followed at λ_{ex}=370 nm, λ_{em}=480 nm (the wavelengths of maxima absorption and emission of 2LZnNd). For the steady-state fluorescence anisotropy experiment, the concentration of 2LZnNd was kept at 2.0 μM. The concentrations of BSA is ranging from 0 to 10 μM.

UV absorbance measurement

UV-visible absorption spectra of 2.0 μM of free 2LZnNd in PBS (pH 7.4±0.1, 0.2% of DMF) as well as the UV-visible absorption spectra of 2LZnNd/BSA complexes (equal molar ratio) were recorded on a TU-1901 UV-Vis spectrometer at room temperature (Puxi Analytic Instrument Ltd. of Beijing, China) from 200 to 350 nm.

CD measurement

The CD spectra were recorded on a J-810-150S Spectropolarimeter (Jasco, Tokyo, Japan), using a cylindrical cuvette with 0.1 cm path length at room temperature under constant nitrogen flush. The CD profiles were obtained employing a scan speed of 200 nm/min and signal averaged for three successive scans. Appropriate baseline corrections in the CD spectra were made. The CD measurements of BSA in the absence and presence of 2LZnNd (1:1, 1:5, 1:10) were made in the range of 260–190 nm. For the CD experiment, the concentration of BSA was kept at 2.0 μM. Far-CD spectra were recorded from 200 to 250 nm in 0.1 M PBS (pH 7.4±0.1), at room temperature.

Results and discussion

Interaction of 2LZnNd with BSA and fluorescence quenching mechanism

Fluorescence quenching efficiency and aspects of the quenching mechanism of the BSA excited state by 2LZnNd were studied by steady-state fluorescence measurements. Fluorescence spectroscopy is useful to obtain local information about the conformational and dynamic changes of protein. The quenching of fluorescence is known to occur mainly by a collisional process (dynamic quenching) and/or formation of a complex between quencher and fluorophore (static quenching) [27]. Here we are interested in knowing whether 2LZnNd form a complex with BSA and upon which the quenching mechanism acts. The effect of 2LZnNd on BSA fluorescence intensity is shown in Fig. 2, from which we can see clearly that BSA had a strong fluorescence emission band around 345 nm by fixing the excitation wavelength at 285 nm, and the fluorescence intensity of BSA was quenched drastically when 2LZnNd was added. The fluorescence intensity of 2LZnNd was nearly zero compared with BSA in the wavelength range of 290–450 nm upon excitation at 285 nm (Fig. 2, line L)

The fluorescence quenching data were plotted as relative fluorescence intensity (RFI=F/F_0) versus 2LZnNd concentration. Fluorescence quenching is described by the well-known Stern–Volmer equation [27]:

$$F_0/F = 1 + k_q\tau_0[Q] = 1 + K_{SV}[Q] \quad (3)$$

Where F_0 and F are the fluorescence intensities absence and presence of quencher, k_q is the bimolecular quenching rate constant, τ_0 is the lifetime of the fluorescence in the absence of quencher [28, 29], [Q] is the concentration of the quencher, and K_{SV} is the Stern–Volmer quenching constant. Hence the above equation could be applied to determine K_{SV} by linear regression of a plot of F_0/F against [Q].

To evaluate the dilution effect by buffer solution, the measurements of BSA titrated by buffer were performed. It was observed that the fluorescence spectra of BSA almost had no change during the buffer titration proceeding (data not shown). The quantitative analysis of the binding of

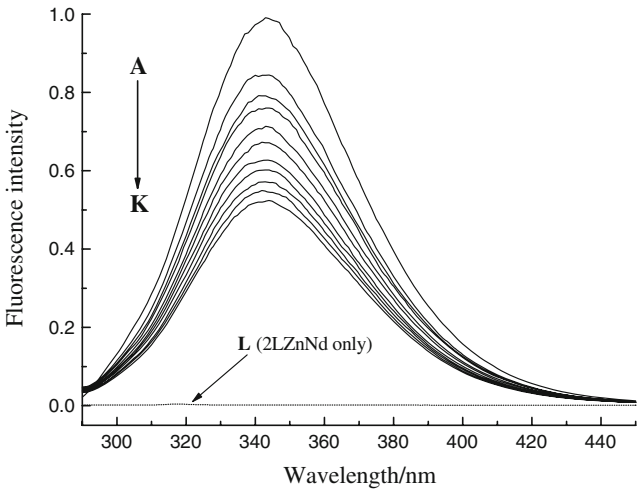

Fig. 2 Emission spectra of BSA in the presence of various concentrations of 2LZnNd

2LZnNd to BSA was carried out using the fluorescence quenching at various temperatures as shown in Fig. 3. The calculation of K_{SV} from Stern–Volmer plots (Fig. 3 A) demonstrated that varying temperatures have a moderate effect on fluorescence quenching by 2LZnNd. Table 1. gives the calculated K_{SV} at each temperature studied, while the results show that the Stern–Volmer quenching constant K_{SV} is inversely correlated with temperature, which indicates that the probable quenching mechanism of a 2LZnNd–BSA binding reaction is initiated by compound formation rather than by dynamic collision. Therefore, the quenching data were then analyzed according to the modified Stern–Volmer equation [30]:

$$F_0/\Delta F = 1/f_a K_a[Q] + 1/f_a \quad (4)$$

In the present case, ΔF is the difference in fluorescence in the absence and presence of the quencher at concentration $[Q]$, f_a is the mole fraction of solvent-accessible fluorophore, and K_a is the effective quenching constant for the accessible fluorophores [31], which are analogous to associative binding constants for the quencher-acceptor system [32, 33]. The dependence of $F_0/\Delta F$ on the reciprocal value of the quencher concentration $[Q]^{-1}$ is linear with the slope equaling the value of $(f_a K_a)^{-1}$. The value $f_a{}^{-1}$ is fixed on the ordinate. The constant K_a is a quotient of the ordinate $f_a{}^{-1}$ and the slope $(f_a K_a)^{-1}$. The modified Stern–Volmer plots are shown in Fig. 3B, and the corresponding quenching constants K_a at different temperatures are shown in Table 1. The decreasing trend of K_a with increasing temperature is in accordance with K_{SV}'s dependence on temperature, which indicates that the fluorescence quenching is caused by a specific interaction, and the quenching is mainly arisen from static quenching by complex formation [27]. Moreover, the UV-vis absorption spectrum of BSA, 2LZnNd and the 2LZnNd–BSA system (data not shown) are different obviously. This result confirmed that static quenching is the mainly quenching mechanism.

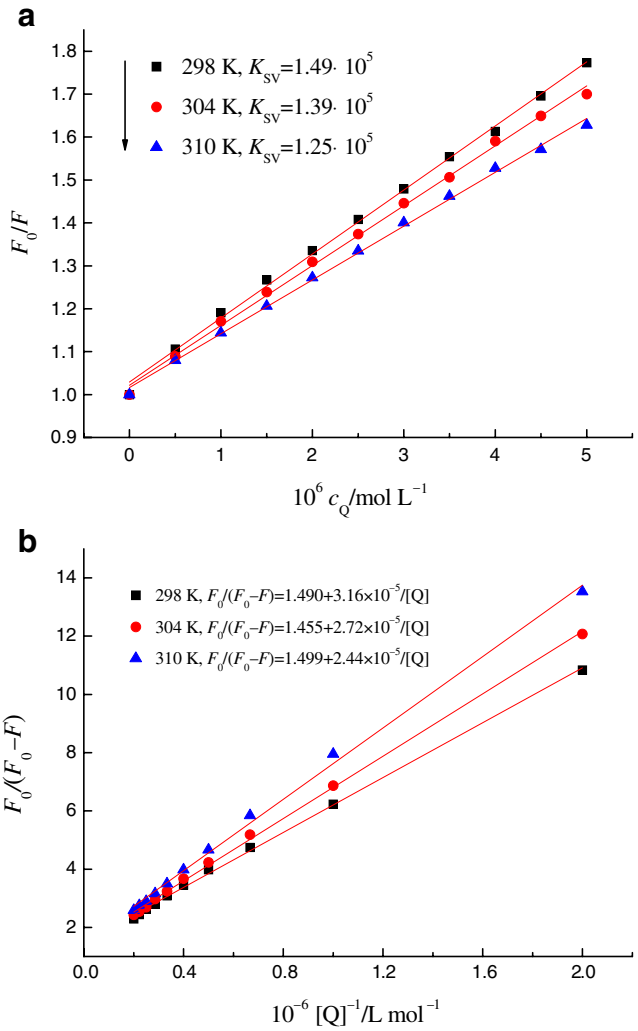

Fig. 3 Stern–Volmer plots (**a**) and modified Stern–Volmer plots (**b**) for the quenching of BSA by 2LZnNd at different temperatures

Motional information of 2LZnNd

Fluorescence anisotropy measurements can give details about an association or binding phenomenon, the technique has been employed to gather additional evidences in support of the interaction of the probe with the native albumin proteins [34, 35]. We have measured the fluorescence anisotropy of 2LZnNd binding to BSA as a function of protein concentration. Figure 4 presents the variation of the fluorescence anisotropy (r) of 2LZnNd (480 nm emission and 370 nm excitation) as a function of protein concentration for BSA. The plot shows a marked increase in the anisotropy value with increasing concentration of BSA, which reflects that the rotational diffusion of 2LZnNd is restricted significantly in the microenvironments of BSA [36]. Figure 4 further reveals that with increasing BSA concentrations, fluorescence anisotropy value increases rapidly at the beginning (up to 4×10^{-6} M) and then levels off gradually. A similar observation has also been reported

Table 1 Stern–Volmer quenching constants of the system of 2LZnNd–BSA at different temperatures

T/K	Stern–Volmer method			Modified Stern–Volmer method		
	10^{-5} K/M^{-1}	R^a	SD^b	10^{-5} K/M^{-1}	R^a	SD^b
298	1.49	0.9976	0.0016	3.15	0.9974	0.069
304	1.39	0.9977	0.0014	2.72	0.9990	0.047
310	1.25	0.9987	0.0098	2.44	0.9993	0.046

[a] R is the correlation coefficient
[b] SD is standard deviation

by Chakrabarty et al. [36]. Increase in anisotropy could be due to decreased Brownian motion or energy transfer between identical chromophores. The high anisotropy value (r=0.17) suggests that 2LZnNd is binding at a motional restricted site on BSA, whose binding site will discuss subsequently.

The binding interaction force between 2LZnNd and BSA

In general, the interaction forces between endogenous or exogenous ligands and biological macromolecules may include electrostatic interactions, multiple hydrogen bonds, van der Waals interactions, hydrophobic, and steric contacts within the antibody-binding site [37]. Ross [38] summed up the thermodynamic laws for estimating the type of the binding force between organic micro-molecule and biological macromolecule. In order to elucidate the interaction between 2LZnNd and BSA, the thermodynamic parameters were calculated from the van't Hoff plots. The temperatures used were 298 K, 304 K, and 310 K. It can be seen from Fig. 5 that there was a good linear relationship between $\ln K_a$ and $1/T$. The enthalpy change (ΔH) is calculated from the slope of the van't Hoff relationship. The free energy change (ΔG) is then estimated from the equation:

$$\Delta G = \Delta H - T\Delta S = -RT\ln K_a \tag{5}$$

Table 2. shows the values of ΔH and ΔS obtained for the binding site from the slopes and ordinates at the origin of the fitted lines. The negative values of free energy (ΔG) support the assertion that the binding process is spontaneous. The negative enthalpy (ΔH) and positive entropy (ΔS) values of the interaction of 2LZnNd and BSA indicate that the electrostatic interactions played a major role in the binding reaction [38].

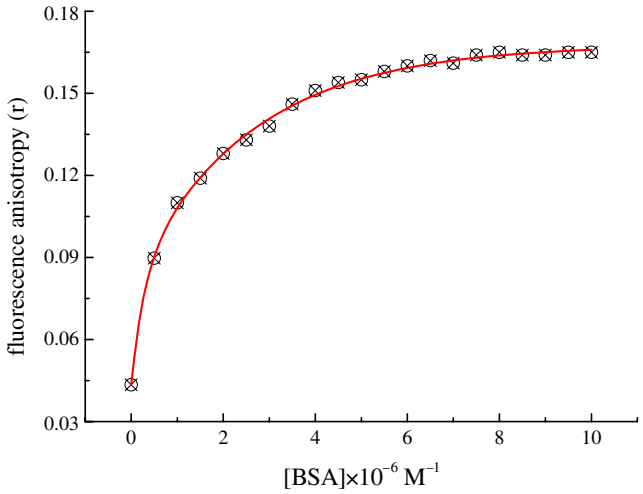

Fig. 4 Variation of fluorescence anisotropy (r) of 2LZnNd with increasing concentrations of BSA, pH 7.4, at room temperature

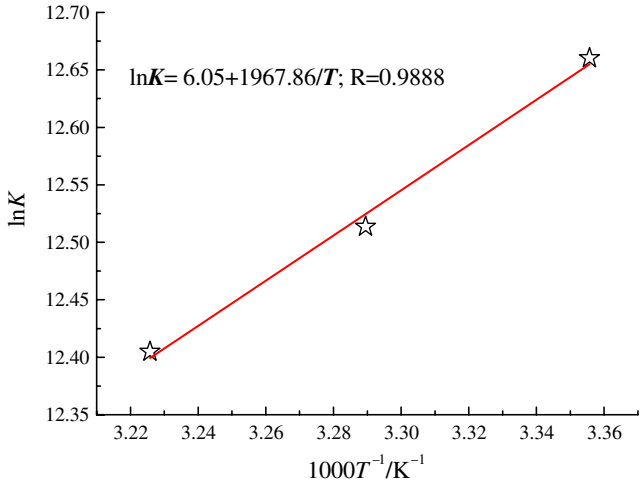

Fig. 5 Van't Hoff plot for the interaction of BSA and 2LZnNd in PBS, pH 7.40

Energy transfer between BSA and 2LZnNd

The distance r between the donor and acceptor can be calculated according to Förster's energy transfer theory. According to this theory, the efficiency of energy transfer between the donor and acceptor, E, could be calculated by the following equation [39, 40]:

$$E = 1 - F/F_0 = R_0^6/\left(R_0^6 + r^6\right) \tag{6}$$

Where r is the distance between the donor and acceptor, R_0 is the critical distance when the efficiency of transfer is 50% and can be calculated by the following equation:

$$R_0^6 = 8.79 \times 10^{-25} K^2 n^{-4} \phi J \tag{7}$$

In Eq. 7, K^2 is the space factor of orientation, n is the refracted index of medium, ϕ is the fluorescence quantum yield of the donor, and J is the effect of the spectral overlap between the emission spectrum of the donor and the absorption spectrum of the acceptor (Fig. 6), which could be calculated by the equation:

$$J = \int_0^\infty F(\lambda)\varepsilon(\lambda)\lambda^4 \mathrm{d}\lambda \Big/ \int_0^\infty F(\lambda)\mathrm{d}\lambda \tag{8}$$

Where $F(\lambda)$ is the corrected fluorescence intensity of the donor in the wavelength range λ to $\lambda + \Delta\lambda$; $\varepsilon(\lambda)$ is the extinction coefficient of the acceptor at λ.

In the present case, K^2=2/3, n=1.36 and ϕ=0.15 [41]. According to the Eqs. 6–8, we could calculate that E=0.32, R_0=3.01 nm and r=3.41 nm. Both the absolute value of the average distance r between the donor fluorophore and the acceptor on the 2−8 nm range [42] and the fulfillment of the required condition, $0.5R_0 < r < 1.5R_0$, converge to indicate that energy transfer from BSA to 2LZnNd occurs with high probability [43]. It also suggested that the binding of

Table 2 Thermodynamic parameters of the system of 2LZnNd–BSA at different temperatures

pH	*T*/K	10^{-5} *K*/M^{-1}	Δ*H*/kJ mol^{-1}	Δ*G*/kJ mol^{-1}	Δ*S*/J mol^{-1} K^{-1}	*R*[a]	SD[b]
7.4	298	3.15	−16.36	−31.35	43.48	0.9888	0.018
	304	2.72		−31.65			
	310	2.44		−31.95			

[a] *R* is the correlation coefficient for the van't Hoff plots;
[b] SD is the standard deviation for the van't Hoff plots.

2LZnNd to BSA is through energy transfer, which is also accord with the electrostatic interaction mechanism.

Confirming the active sites location of 2LZnNd on BSA

As the data in the preceding discussion do not allow us to give the precise binding sites location of 2LZnNd on the protein, competitive displacement experiments were also carried out using site-specific probes, warfarin and ibuprofen [44–46] (Molecular structure in Fig. 1) by fluorescence quenching method. Most studies of the two site markers, by means of equilibrium dialysis, found that warfarin mostly located in site I on the BSA, ibuprofen possesses one high-affinity sites in site II and several low-affinity binding sites in site I, respectively [45, 46]. The binding constants of the high-affinity site are in the range 8.9×10^4~3.4×10^5 M^{-1} for warfarin binding to BSA, 3.0×10^5~3.6×10^6 M^{-1} for racemic ibuprofen [47].

To identify the binding site location of 2LZnNd on the region of BSA, the binary mixture of warfarin–BSA or ibuprofen–BSA were titrated with 2LZnNd. The fluorescences spectra were recorded upon excitation at 285 nm, and the quenching data were analyzed according to the modified Stern–Volmer equation (Eq. 4). It is observed that, the effective quenching constant K_a of equimolar concentrations (2 μM) of ibuprofen–BSA complex was quickly decreased from 2.43×10^5 to 2.0×10^4 M^{-1} (Fig. 7) when 2LZnNd was added into the ibuprofen–BSA complex, while the K_a value of warfarin–BSA complex titrated by 2LZnNd was not affected (2.43×10^5 vs 2.47×10^4 M^{-1}). Considering that the binding constant for ibuprofen binding to BSA (3.0×10^5~3.6×10^6 M^{-1}, larger than that of 2LZnNd) Putting the facts that the interaction is slightly exothermic [48], and different enantioselectivities [49], it is evident that 2LZnNd does bind at the region of site II (subdomain IIIA) and is buried in this hydrophobic pocket.

Conformation investigation

To ascertain the possible influence of 2LZnNd binding on the secondary structure of BSA, we have performed far-UV CD spectroscopy of BSA in the absence and in the presence of 2.0 to 20.0×10^{-6} M 2LZnNd (molar ratios of BSA to 2LZnNd were 1:0, 1:1, 1:5 and 1:10). Consistent with the literature, the CD spectra of BSA exhibited two negative bands in the UV region at 208 and 222 nm, characteristic of α-helical structure of protein. The reasonable explanation is that the negative peaks between 208 and 209 and 222 and 223 nm both contribute to the $n\rightarrow\pi^*$ transfer for the peptide bond of the R-helix. The CD results were expressed

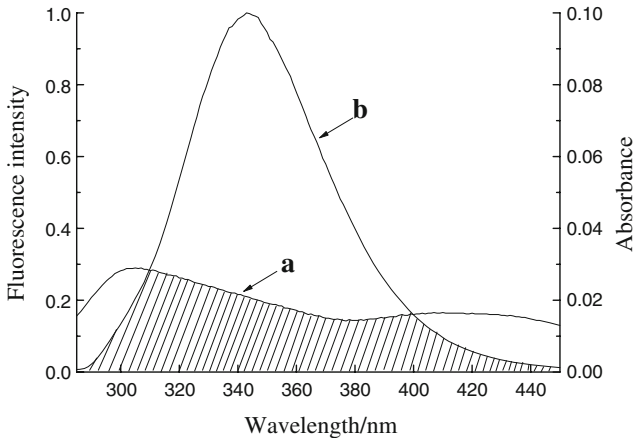

Fig. 6 Spectral overlap of 2LZnNd absorption (**a**) with BSA fluorescence (**b**)

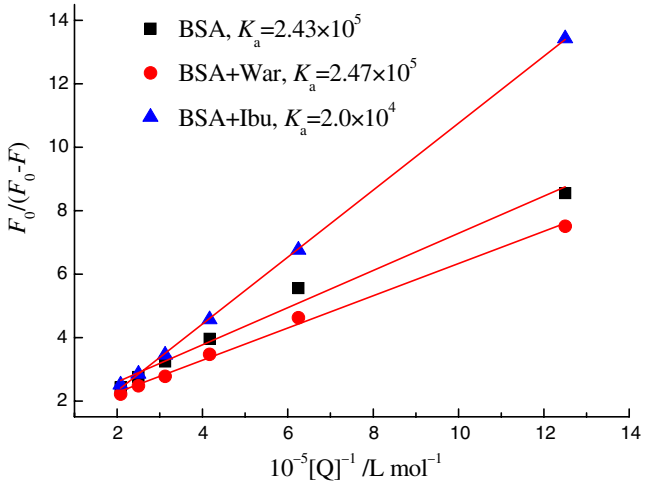

Fig. 7 CD spectra of the 2LZnNd–BSA system at pH 7.40

in terms of mean residue ellipticity (MRE) in deg cm^2 d mol^{-1} according to the following equation:

$$\mathrm{MRE} = \text{Observed } CD(mdeg)/C_p nl \times 10 \quad (9)$$

Where C_p is the molar concentration of the protein, n the number of amino acid residues (583 for BSA) and l is the path length (0.1 cm). The α-helical contents of free and combined BSA were calculated from MRE values at 208 nm using the equation:

$$\alpha - \mathrm{helix}(\%) = (-\mathrm{MRE}_{208} - 4,000)/(33,000 - 4,000) \quad (10)$$

as described by Lu et al. [50]. Where MRE_{208} is the observed MRE value at 208 nm, 4,000 is the MRE of the β-form and random coil conformation cross at 208 nm and 33,000 is the MRE value of a pure α-helix at 208 nm. From the above equation, the α-helicity in the secondary structure of BSA was determined. Figure 8 presents a set of representative CD spectra for the 2LZnNd–BSA system, and the inset shows the helicity of BSA versus the concentration of 2LZnNd at 208 and 222 nm. As can be seen, the helicity of BSA decreased significantly with increasing the concentration of 2LZnNd.

Furthermore, in order to quantify the different types content of secondary structures, far-UV CD spectra have been analyzed by the algorithm SELCON3, with known precise secondary structures (43 mode proteins) used as the reference set [51, 52]. The values of secondary structures for BSA in the absence and presence of 2LZnNd are shown in Table 3. A decreasing tendency of the α-helices content and an increasing tendency of β-strands, turn, and unordered structures contents were estimated at high 2LZnNd concentration (Table 3). As known, the secondary structure contents are related close to the biological activity of the protein, thus a decrease in α-helical from 61.2% to 47.9% meant the loss of the biological activity of BSA upon interaction with the highest concentration of 2LZnNd.

Additional evidence regarding the conformational changes of BSA in presence of 2LZnNd came from the three-dimensional fluorescence measurement. In Fig. 9, peak 1 is mainly reveals the spectral behavior of tryptophan and tyrosine residues, and the maximum emission wavelength and the fluorescence intensity of the residues are in close correlation of their microenvironment's polarity [53]. Figure 9 and Table 4. show that after the addition of 2LZnNd the maximum emission wavelength had a slight blue shift and the relative fluorescence intensity of BSA weakened from 224.3 to 202.0. This suggested a less polar environment of both residues and almost all the hydrophobic amino acid residues of BSA are buried in the hydrophobic pocket. Less polar environment meant that the binding position between 2LZnNd and BSA locate within this hydrophobic pocket, the addition of 2LZnNd changed the polarity of this hydrophobic microenvironment and the conformation of BSA. All these findings were consistent with the results of competitive displacement experiments and CD spectra.

Besides peak 1, we found another new interesting fluorescence peak (peak 2, λ_{ex}=225.0 nm, λ_{em}=345.4 nm). we assume that peak 2 may mainly exhibit the fluorescence spectra behavior of polypeptide backbone structures, which is mainly caused by the transition of $P \rightarrow P^*$ of BSA's characteristic polypeptide backbone structure C=O. So In the presence of 2LZnNd (molar ratio of BSA to 2LZnNd was 1:1), the fluorescence intensity of peak 2 decreases rapidly from 157.8 to 4.4, which indicates that the interaction of 2LZnNd with BSA induced the unfolding of the polypeptides of protein and conformational change of the protein [54]. All these phenomenon and analyzing of peak 1 and peak 2 revealed that the binding of

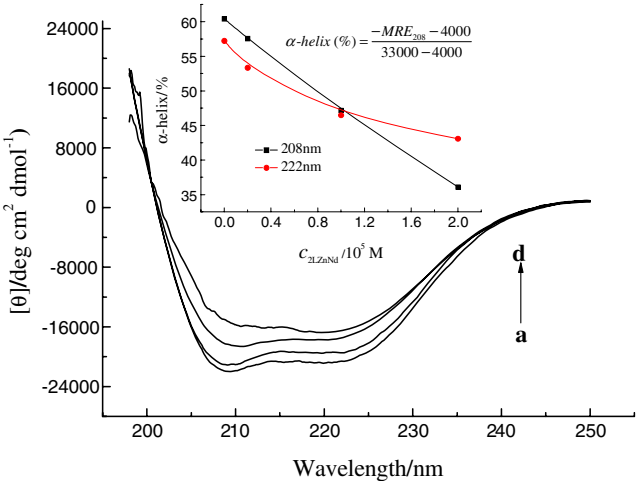

Fig. 8 Three-dimensional fluorescence spectra of BSA (**a**) and 2LZnNd–BSA complex (**b**)

Table 3 Fractions of different secondary structures determined by SELCON3[a]

molar ratio [2LZnNd]:[BSA]	Percentage of secondary structure					
	α-helix		β-strand		Turn	Unordered
	α_R	α_D	β_R	β_D		
0:1	41.2	20.0	2.7	2.8	12.7	20.6
1:1	38.8	19.9	3.2	3.4	14.3	21.2
5:1	33.6	18.8	5.0	4.7	16.4	24.4
10:1	29.7	18.2	5.8	5.3	18.6	25.6

[a] The subscripts "R" and "D" represent "ordered" and "disordered", respectively.

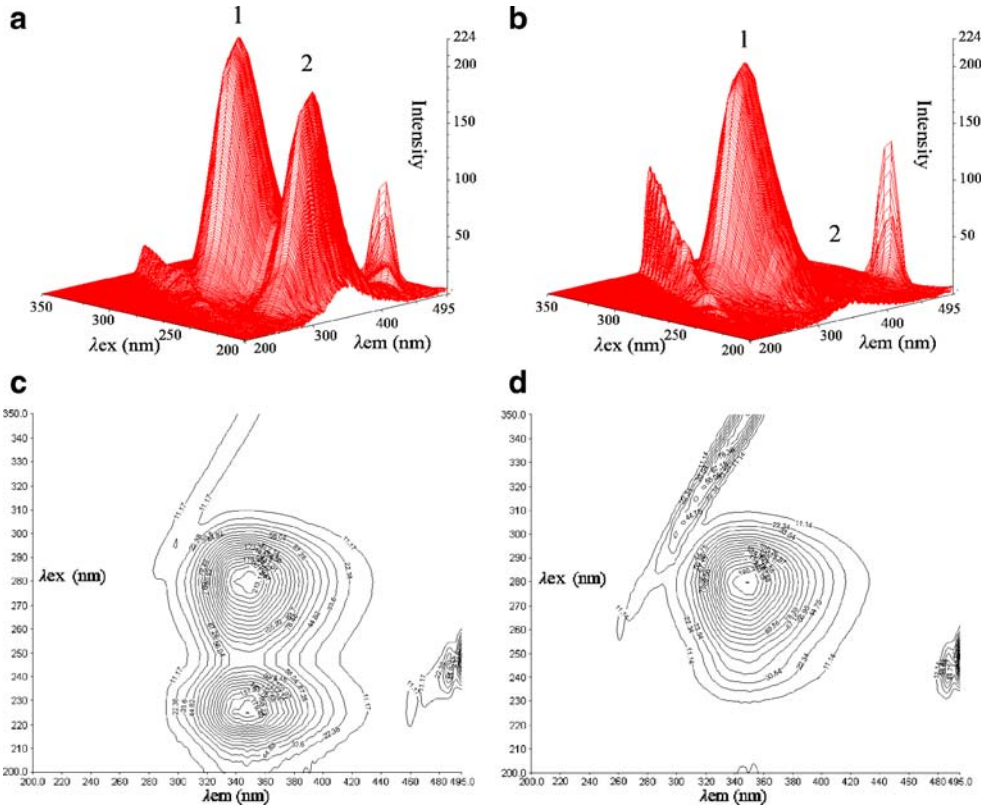

Fig. 9 Contour spectra of BSA (**a**) and 2LZnNd–BSA complex (**b**)

2LZnNd to BSA induced some micro-environmental and conformational changes in BSA.

Conclusions

In this paper, the interaction between 2LZnNd and BSA was investigated by fluorescence quenching spectrum, UV-vis spectrum, CD, and three-dimensional fluorescence spectrum. The Stern–Volmer quenching constant K_{sv} and corresponding thermodynamic parameters ΔH, ΔG and ΔS were calculated. The negative enthalpy (ΔH) and positive entropy (ΔS) values of the interaction of 2LZnNd and BSA indicate that the electrostatic interactions played a major role in the binding reaction. The distance r between donor (BSA) and acceptor (2LZnNd) was calculated to be 3.41 nm according to Förster's energy transfer theory. Competitive displacement experiments reveal that the binding location of 2LZnNb to BSA is in the hydrophobic pocket of site II. The effect of 2LZnNd on the conformation of BSA has been analyzed by CD and three-dimensional fluorescence spectra, the results indicate that the secondary structure of BSA molecules was changed in the presence of 2LZnNd. All these experimental results and theoretical data clarified that 2LZnNd could bind to BSA and could be effectively transported and eliminated in body, which may provide valuable information to the growing concern regarding the biological action of Zn–Nd hetero-bimetallic Schiff base introduced to organism.

Acknowledgements We thank Professor Rick W. K. Wong (Department of Chemistry, Hong Kong Baptist University) for providing 2LZnNd. We gratefully acknowledge financial support of Chinese 863 program (2007AA06Z407), National Natural Science Foundation of China (20873096, 30570015, 20621502), Research Foundation of Chinese Ministry of Education (20068-IRT0543), Natural Science Foundation of Hubei Province (2005ABC002).

Table 4 Three-dimensional fluorescence spectral characteristics of BSA and 2LZnNd–BSA system

Peaks	BSA			2LZnNd–BSA		
	Peak position $\lambda_{ex}/\lambda_{em}$ (nm/nm)	Storkes $\Delta\lambda$ (nm/nm)	Intensity F	Peak position $\lambda_{ex}/\lambda_{em}$ (nm/nm)	Storkes $\Delta\lambda$ (nm/nm)	Intensity F
Fluorescence peak 1	280.0/348.5	68.5	224.3	280.0/346.5	66.5	202.0
Fluorescence peak 2	225.0/345.4	120.4	157.8	225.0/353.9	128.9	4.4

References

1. Zhong X, Yi J, Sun J, Wei HL, Liu WS, Yu KB (2006) Synthesis and crystal structure of some transition metal complexes with a novel bis-Schiff base ligand and their antitumor activities. Eur J Med Chem 41:1090–1092
2. Yang ZY, Yang RD, Li FS, Yu KB (2000) Crystal structure and antitumor activity of some rare earth metal complexes with Schiff base. Polyhedron 19:2599–2604
3. Wang BD, Yang ZY, Wang Q, Cai TK, Crewdson P (2006) Synthesis, characterization, cytotoxic activities, and DNA-binding properties of the La(III) complex with Naringenin Schiff-base. Bioorg Med Chem 14:1880–1888
4. Anacona JR, Bastardo E, Camus J (1999) Manganese(II) and palladium(II) complexes containing a new macrocyclic Schiff base ligand: antibacterial properties. Transition Met Chem 24 (4):478–480
5. Raman N, Kulandaisamy A, Thangaraja C (2004) Structural characterisation and electrochemical and antibacterial studies of Schiff base copper complexes. Transition Met Chem 29(2):129–135
6. Chaviara AT, Cox PJ, Repana KH, Papi RM, Papazisis KT, Zambouli D, Kortsaris AH, Kyriakidis DA, Bolos CA (2004) Copper(II) Schiff base coordination compounds of dien with heterocyclic aldehydes and 2-amino-5-methyl-thiazole: synthesis, characterization, antiproliferative and antibacterial studies. Crystal structure of CudienOOCl(2). J Inorg Biochem 98(8):1271–1283
7. Chohan ZH (2001) Praveen M Synthesis, characterization, coordination and antibacterial properties of novel asymmetric 1,1′-disubstituted ferrocene-derived Schiff-base ligands and their Co(II), Cu(II) Ni(II) and Zn(II) complexes, *M. Praveen*. Appl Organomet Chem 15(7):617–625
8. Denardo GL, Mirik GR, Kroger LA, Donnel RTO, Meares CF, Denardo SL (1996) Antibody responses to macrocycles in lymphoma. J Nucl Med 37(3):451–456
9. Chohan ZH, Pervez HY, Rauf A, Scozzafava A, Supuran CT (2002) Antibacterial Co(II), Cu(II), Ni(II) and Zn(II) complexes of thiadiazole derived furanyl, thiophenyl and pyrrolyl Schiff bases. J Enzyme Inhib Med Chem 17(2):117–122
10. Wang Y, Yang ZY, Wang BD (2005) Synthesis, characterization and anti-oxidative activity of cobalt(II), nickel(II) and iron(II) Schiff base complexes. Transition Met Chem 30(7):879–883
11. Jain M, Singh RV (2003) Spectral and antimicrobial studies of organosilicon(IV) complexes of a bidentate Schiff base having nitrogen-nitrogen donor system. Main Group Met Chem 26:237–246
12. Ali MA, Mirza AH, Butcher RJ, Tarafder MTH, Keat TB, Ali AM (2002) Biological activity of palladium(II) and platinum(II) complexes of the acetone Schiff bases of *S*-methyl- and *S*-benzyldithiocarbazate and the X-ray crystal structure of the [Pd $(asme)_2$] (asme = anionic form of the acetone Schiff base of *S*-methyldithiocarbazate) complex. J Inorg Biochem 92:141–148
13. El-Wahab ZHA, El-Sarrag MR (2004) Derivatives of phosphate Schiff base transition metal complexes: synthesis, studies and biological activity. Spectrochim Acta A 60:271–277
14. Chakrabortya J, Piletb G, Fallahc MSE, Ribasc J, Mitra S (2007) Synthesis, characterisation and cryomagnetic studies of a novel homonuclear Nd(III) Schiff base dimmer. Inorg Chem Commun 10(4):489–493
15. Boghaei DM, Farvid SS, Gharagozlou M (2007) Interaction of copper(II) complex of compartmental Schiff base ligand *N*,*N*′-bis (3 -hydroxysalicylidene)ethylenediamine with bovine serum albumin. Spectrochim Acta A 66:650–655
16. Shrivastava HY, Kanthimathi M, Nair BU (1999) Interaction of Schiff base with bovine serum albumin: site-specific photocleavage, biochemical and biophysical research Communications. Biochem Biophys Res Commun 265:311–314
17. Sasnouski S, Zorin V, Khludeyev I, D'Hallewin MA, Guillemin F, Bezdetnaya L (2005) Investigation of Foscan interactions with plasma proteins. Biochim. Biophys. Acta 1725:394–402
18. Hu YJ, Liu Y, Zhao RM, Dong JX, Qu SS (2004) Study of the interaction between monoammonium glycyrrhizinate and bovine serum albumin. J Photochem Photobiol A: Chem 179:324–329
19. Qi ZD, Zhou B, Xiao Q, Shi C, Liu Y, Dai J (2008) Interaction of rofecoxib with human serum albumin: Determination of binding constants and the binding site by spectroscopic methods. J Photochem Photobiol A: Chem 193(2–3):81–88
20. He XM, Carter DC (1992) Atomic structure and chemistry of human serum albumin. Nature 358:209–215
21. Dockal M, Carter DC, Rűker F (2000) Conformational transitions of the three recombinant domains of human serum albumin depending on pH. J Biol Chem 275(5):3042–3050
22. Olson RE, Christ DD (1996) Plasma protein binding of drugs. Annu Rep Med Chem 31:327–337
23. Wang YQ, Zhang HM, Zhang GC (2006) Studies of the interaction between palmatine hydrochloride and human serum albumin by fluorescence quenching method. J Pharm Biomed Anal 41:1041–1046
24. Brockhinke A, Plessow R, Kohse-Höinghaus K, Herrmann C (2003) Structural changes in the Ras protein revealed by fluorescence spectroscopy. Phys Chem Chem Phys 5:3498–3506
25. Lo WK, Wong WK, Guo JP, Wong WY, Li KF, Cheah KW (2004) Synthesis, Structures and Luminescent Properties of New Heterobimetallic ZN-4f Schiff Based Complexes. Inorg Chim Acta 357:4510–4521
26. Bentley KL, Thompson LK, Klebe RJ, Horowitz PM (1985) Fluorescence polarization: a general method for measuring ligand binding and membrane microviscosity. BioTechniques 3:356–366
27. Lakowicz JR (2006) Principles of fluorescence spectroscopy 3rd ed. Plenum, New York
28. Eftink MR (1991) Fluorescence quenching reactions: probing biological macromolecular structures. Plenum, New York
29. Lakowica JR, Weber G (1973) Quenching of fluorescence by oxygen, a probe for structural fluctuations in macromolecules. Biochemistry 12:4161–4170
30. Lehrer SS (1971) The quenching of the tryptophyl fluorescence of model compounds and of lysozyme by iodide ion. Biochemistry 10:3254–3263
31. Wilson CJ, Copeland RA (1997) Spectroscopic characterization of arrestin interactions with competitive ligands: study of heparin and phytic acid binding. J Protein Chem 16:755–763
32. Murphy CB, Zhang Y, Troxler T, Ferry V, Martin JJ, Jones WE (2004) Probing Förster and Dexter energy-transfer mechanisms in fluorescent conjugated polymer chemosensors. J Phys Chem B 108:1537–1543
33. Watt RM, Voss EW (1979) Solvent perturbation of the fluorescence of fluorescein bound to specific antibody. J Biol Chem 254:1684–1690
34. Kusba J, Lakowicz JR (1999) Definition and properties of the emission anisotropy in the absence of cylindrical symmetry of emission field: application to the light quenching experiments. J Chem Phys 111:89–99
35. He WY, Li Y, Si HZ, Dong YM, Sheng FL, Yao XJ, Hu ZD (2006) Molecular modeling and spectroscopic studies on the binding of guaiacol to human serum albumin. J Photochem Photobiol A 182:158–167
36. Chakrabarty A, Mallick A, Haldar B, Das P, Chattopadhyay N (2007) Binding interaction of a biological photosensitizer with serum albumins: a biophysical study. Biomacromolecules 8:920–927

37. Leckband D (2000) Measuring the forces that control protein interactions. Annu Rev Biophys Biomol Struct 29:1–26
38. Ross PD, Subramanian S (1981) Thermodynamics of protein association reaction: forces contribution to stability. Biochemistry 20:3096–3102
39. Sklar LA, Hudson BS, Simoni RD (1977) Conjugated polyene fatty acids as fluorescent probes: synthetic phospholipid membrane studies. Biochemistry 16:819–828
40. Stryer L (1978) Fluorescence energy transfers as a spectroscopic ruler. Annu Rev Biochem 47:819–846
41. Long C, King EJ, Sperry WM (1961) Biochemists' Handbook. E. & F. N. Spon Ltd, London
42. Valeur B, Brochon JC (1999) New Trends in Fluorescence Spectroscopy. Springer Press, Berlin
43. Valeur B (2001) Molecular Fluorescence: Principles and Applications. Wiley Press, New York
44. Epps DE, Raub TJ, Kézdy FJ (1995) A general wide-range spectrofluorometric method for measuring the site-specific affinities of drugs toward human serum albumin. Anal Biochem 227:342–350
45. Kosa T, Maruyama T, Otagiri M (1997) Species differences of serum albumin: I. Drug binding sites. Pharm Res 14:1607–1612
46. Bos OJM, Remijn JPM, Fischer MJE, Wilting J, Janssen LHM (1988) Location and characterization of the warfarin binding site of human serum albumin: a comparative study of two large fragments. Biochem Pharmacol 37:3905–3909
47. Epps DE, Raub TJ, Kézdy FJ (1995) A general, wide-rage spectrofluorometric method for measuring the site-specific affinities of drugs toward human serum albumin. Anal Biochem 227 (2):342–350
48. Maes V, Engelborghs Y, Hoebeke J, Maras Y, Vercruyysse A (1981) Fluorimetric analysis of the binding of warfarin to human serum albumin. Mol Pharmacol 21:100–107
49. Noctor TAG, Pham CD, Kaliszan R, Wainer IW (1992) Stereochemical aspects of benzodiazepine binding to human serum albumin. I. Enantioselective high performance liquid affinity chromatography examination of chiral and achiral binding interactions between 1,4-benzodiazepines and human serum albumin. Mol Pharmacol 42:506–511
50. Lu ZX, Cui T, Shi QL (1987) Application of Circular Dichroism and Optical Rotatory Dispersion in Molecular Biology 1st ed. Science, Beijing
51. Sreerama N, Woody RW (1993) A self-consistent method for the analysis of protein secondary structure from circular dichroism. Anal Biochem 209:32–44
52. Whitmore L, Wallace BA (2004) DICHROWEB, an online server for protein secondary structure analyses from circular dichroism spectroscopic data. Nucleic Acids Res 32:W668–W673
53. Zhang YZ, Zhou B, Liu YX, Zhou CX, Ding XL, Liu Y (2008) Fluorescence study on the interaction of bovine serum albumin with *p*-aminoazobenzene. J Fluoresc 18:109–118
54. Tian JN, Liu JQ, Hu ZD, Chen XG (2005) Interaction of wogonin with bovine serum albumin. Bioorg Med Chem 13:4124–4129